High-resolution cavity bunch arrival-time monitor for charges less than 1 pC

Chuangye Song, Yanqing Jia, Zhuoyuan Liu, Yingchao Du, and Wenhui Huang*

Department of Engineering Physics, Tsinghua University Beijing, Beijing 100084, People's Republic of China and Key Laboratory of Particle and Radiation Imaging, Tsinghua University, Ministry of Education, Beijing 100084, People's Republic of China

(Received 20 September 2022; accepted 4 January 2023; published 18 January 2023)

Pump-probe experiments using x-ray pulses or MeV ultrafast electrons as probes are important for studying ultrafast dynamic processes at the atomic level. Increasing demand is being focused on ultrashort x-ray pulses and electron pulses to research processes down to a few femtoseconds. Due to the limitation of the space charge force, only low charge electron bunches with critical synchronization can achieve such short pulses. A high-precision beam arrival-time monitor for the low charge is especially important. In this paper, a low Q_l cavity with high sensitivity is designed to measure the arrival time of charges below 1 pC. The pickup is particularly optimized with high R/Q at 4.76 GHz to provide the maximum signal, and the cold test results are in good agreement with the simulations. An IQ demodulation scheme is developed for the readout electronics. In the beam tests, the measured resolution of the beam arrival-time monitor is 33.46 fs at 0.5 pC.

DOI: 10.1103/PhysRevAccelBeams.26.012803

I. INTRODUCTION

Ultrafast exploration with the atomic resolution has contributed to many new breakthroughs in chemistry, biology, medicine, and materials science [1,2]. Pump-probe experiments with free-electron lasers (FELs) or ultrafast electron diffraction (UEDs) for microscopic detection of ultrafast dynamic processes are some of the most interesting applications [3,4], which have very high synchronization requirements. Bunch arrival-time measurement with femtosecond precision is essential for these experiments. An accurate measurement of the arrival time can not only help improve these studies but also be used as feedback for machine synchronization to reduce the timing jitter at key locations [5,6].

In recent years, these time-resolved measurements with FELs have had an emerging demand for ultrashort FEL shots [7,8], down to a few femtoseconds. The self-amplified spontaneous emission (SASE) process is essentially determined by the length of the electron bunch [9]. To generate short x-ray pulses, short and low charge electron bunches are now a favorable choice, which may also reduce the machine jitter [10,11]. At FLASH and the European X-Ray Free-Electron Laser Facility (EXFEL), the bunch charge was upgraded to a broad range, from 0.02 to 1 nC [12], and in the low charge mode, the bunch length can be compressed to below 3 fs [13]. For UED facilities, using short electron beams as probes for ultrafast investigations, the bunch length is mainly limited by the space charge force. The beam charge in a UED is also at the hundreds of fC level to achieve short pulses [4,14]. Therefore, a high-resolution beam arrival-time monitor (BAM) for the low charge is increasingly necessary.

Currently, there are some schemes for beam arrival-time measurements, mainly based on the rf cavity with the rf-phase detection method [15] and the amplitude modulation using the Mach-Zehnder (electro-optical) modulator (EOM) [16]. The EOM scheme at FLASH consists of three parts: the high bandwidth rf pickup, the electro-optical unit, and the data acquisition system [5]. The pickup signal induced by the beam is fed into an electro-optical modulator to modulate an external laser pulse train [16]. In this method, the resolution is mainly determined from the steepness of the modulation slope and the laser amplitude jitter of the pulses preceding the first modulation [16]. A temporal resolution of 3 fs@250 pC was reached at EXFEL by using a 40 GHz bandwidth cone-shaped pickup [17]. Since the slope of the pickup signal decreases proportional to the bunch charge, the BAM performance at lower charge rapidly degrades [18]. To reach the target set for 1 pC, more designs were proposed, such as reducing the beampipe aperture and a new 90 GHz cone-shaped pickup [19–21].

*huangwh@mail.tsinghua.edu.cn

The resonant detection scheme utilizes an rf phase cavity to extract an accurate bunch arrival time. A series of eigenmodes is excited in the cavity by the passing bunches [22]. For a cylindrical cavity, the TM_{010} monopole mode signal is proportional to the beam charge and is insensitive to the beam offset [23]. Precise bunch charge and arrival-time information can be obtained from the amplitude and phase of the TM_{010} mode signal by mixing it with the reference clock. Compared with the EOM detection scheme, this scheme also has the potential to achieve sub-10 fs resolution [24]. Cavity beam arrival-time monitors are currently used in many facilities [25–28]. The best resolution has been reported as 13 fs@250 pC and 27 fs@20 pC in low charge mode with a 2806 MHz phase cavity at the Linac Coherent Light Source (LCLS) [26]. For low charge bunches, the key point is to design a highly sensitive pickup. The energy transferred to a cavity when a beam passes through it is proportional to the R/Q of the pickup [23]. The R/Q value depends only on the geometry. The coupling constant β is also a significant parameter that defines the strength of the coupling between the cavity and the external circuit. An overcoupling setting is a better choice to extract more energy from the cavity. To maximize the signal, the cavity needs a high R/Q and overcoupling structure. A cavity BAM for charges well below 1 pC is designed for the relativistic electron gun for atomic exploration. It comprises a 3.025 GHz cavity with an optimized R/Q of 236 Ω [29]. Publication of the pickup measurements and beam experiments is awaited. To obtain high precision of the cavity BAM at low charges, we developed a 4.76 GHz cavity and achieved the maximum R/Q at the resonant frequency with the CST eigenmode solver [30]. The coupling structure was also carefully optimized since it determines the decay constant related to the sampling rate of electronics. Beam experiments were performed, and a high-resolution cavity BAM for charges less than 1 pC was realized for the first time.

Our work is organized as follows: In Sec. II, the design process, simulation, and cold test results are introduced, mainly focusing on R/Q optimization. Section III describes the scheme and performance of the readout electronics. The BAM resolution measurements are presented in Sec. IV.

II. CAVITY DESIGN AND TEST RESULTS

A cavity BAM usually consists of a pillbox cavity as a pickup. When a beam passes through the cavity, the electromagnetic field of a series of eigenmodes is excited, called the wakefield effect [23]. Considering a beam bunch of charge q and assuming a Gaussian distribution in the beam direction with beam size σ_z, the output voltage signal V_{out} of the TM_{010} mode is expressed as follows:

$$V_{\text{out}} = \frac{\omega q}{2}\sqrt{\frac{Z}{Q_{\text{ext}}}\frac{R}{Q}}\exp\left(-\frac{\omega^2\sigma_z^2}{2c^2}\right), \tag{1}$$

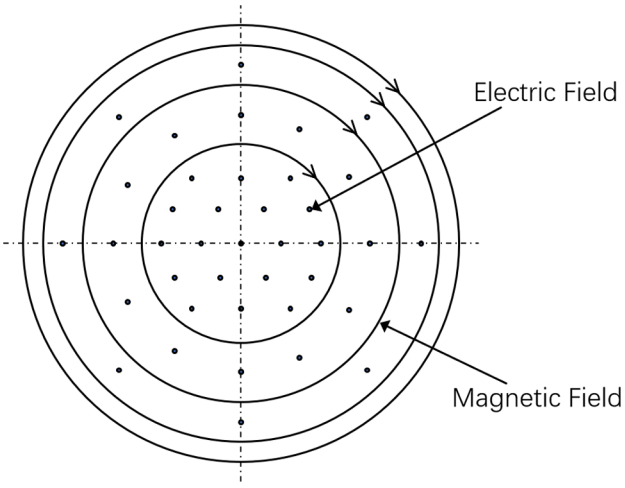

FIG. 1. Electromagnetic fields of the monopole mode.

where c is the speed of light, Z is the characteristic impedance, ω is the frequency, Q_{ext} is the external quality factor, which is mostly determined by the coupling structure, and R/Q is the normalized shunt impedance. R/Q is proportional to the energy lost in the pickup by a beam and solely depends on the cavity shape. Therefore, it is a critical parameter for optimization. For the monopole mode, R/Q is calculated as

$$\left(\frac{R}{Q}\right)_{010} = \frac{2J_0^2(\frac{j_{01}x}{a})LT^2}{\omega\varepsilon_0\pi J_1^2(j_{01})a^2} \tag{2}$$

where x is the beam offset, a is the cavity diameter, L is the cavity length, T is the transit time factor, J_0 is the zeroth-order Bessel function, j_{01} is the first root, and J_1 is the first-order Bessel function. According to the properties of the J_0 function, this R/Q value is a constant when the beam is near the cavity center [23]. The fields for the TM_{010} mode are shown in Fig. 1 [31].

A. Cavity design process

The resonant frequency is an important factor for the BAM. For low charge operation, the choice of frequency should avoid any background due to the dark current to achieve the best performance. The dark current is mainly caused by the high field in the electron gun and distributes in every rf period [32]. The Tsinghua Accelerator Laboratory utilizes a 1.6 cell rf gun operated at 2.856 GHz [33]. When the frequency shifts away from 2.856 GHz and its multiples, the noise caused by the dark current rapidly decreases. Also considering the electronics and the cutoff frequency, 14.65 GHz for a 6-mm radius beam pipe, the frequency is intentionally designed to be 4.76 GHz.

The pickup was simulated with the electromagnetic solver in CST Microwave Studio [30], and the R/Q was investigated as a figure of merit in the optimization. The pickup was chosen as a coaxial reentrant cavity because of

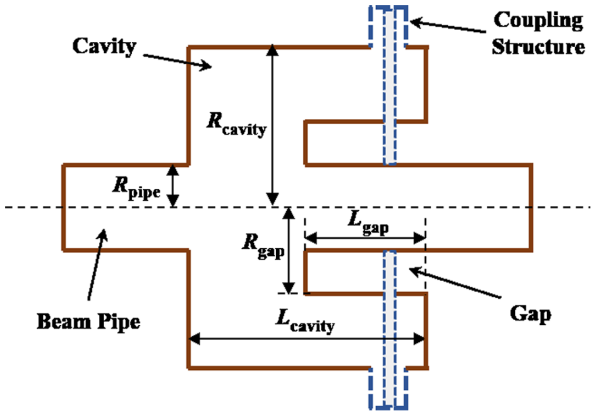

FIG. 2. Schematic cross section of the cavity. In the R/Q optimization process, the cavity is built without the coupling structure (the blue dotted line).

its mechanical simplicity. The desired frequency can be easily reached by tuning the reentrant part. As shown in Fig. 2, the structure is composed of four distinct areas: the beam pipe, reentrant gap, coaxial cylinder, and coupling structure [34]. To simplify the optimization process, the cavity was first built without the coupling structure, which has little influence on the R/Q value. There are five adjustable variables: the pipe radius R_{pipe}, cavity length L_{cavity}, cavity radius R_{cavity}, gap length L_{gap}, and gap radius R_{gap}.

The pipe radius of our beamline usually ranges from 6 to 15 mm, and R_{pipe} is selected to be 6 mm. A small radius can lead to a stronger interaction between the cavity and the electron beam. A parameter sweep was performed over the remaining four variables to optimize the R/Q value. First, given a set of L_{cavity} and R_{cavity}, the maximum R/Q value with the frequency fixed at 4.76 GHz can be found by scanning L_{gap} and R_{gap}. Then, we change the set of L_{cavity} and R_{cavity} and repeat the above process. R/Q values with different sets of cavity length and radius were obtained, as shown in Fig. 3. In this figure, the R/Q value increases with the cavity length and radius. Since the cavity size is limited by the fixed frequency, the maximum R/Q is nearly 300 Ω under the condition of 4.76 GHz. Stainless steel was employed as the pickup material which has low thermal conductivity and simple machining processes. The electrical conductivity of stainless steel is smaller than that of oxygen-free copper, which means a low Q_0 factor.

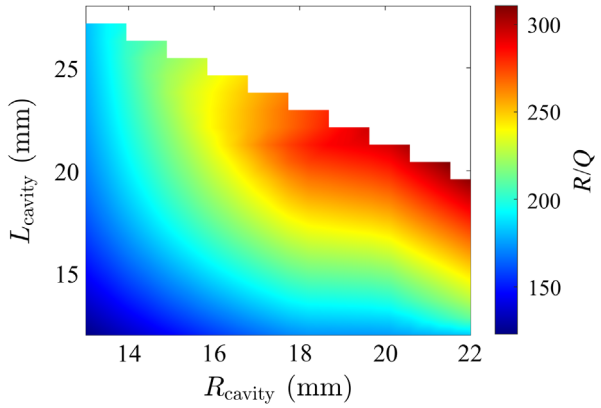

FIG. 3. R/Q variations of the cavity at 4.76 GHz with the cavity length and radius.

Afterward, the coupling structure was added to the model. According to Eq. (1), the voltage signal is inversely proportional to $\sqrt{Q_{\mathrm{ext}}}$. Overcoupling can be achieved by adjusting the position and radius of the coupling hole, that is, a small $\sqrt{Q_{\mathrm{ext}}}$. Finally, magnetic coupling was adopted for the cavity, and antennas were inserted into the wall, as illustrated in Fig. 2. This method ensures good contact and reduces the difficulty of assembly. The radii of the coupling hole and antenna are 1.85 and 0.8 mm, respectively, ensuring a characteristic impedance of 50 Ω. The sensitivity of the pickup was also simulated using the wakefield solver in CST. The charge of the beam was set to 1 pC and the output signal of the port was monitored. The optimized dimensions and simulated parameters are summarized in Table I.

B. Tolerance analysis

Fabrication errors and tolerances may shift the resonance frequency and change the coupling coefficient. An error tolerance study must be conducted to analyze the effect of dimensional errors on rf parameters [35]. As shown in Fig. 4, mechanical errors in three dimensions were simulated to study the effect on f, Q_{ext} and R/Q. The tolerance analysis results obtained with the postprocessing template of the eigenmode solver are shown in Fig. 5. Since these mechanical errors should be at least 2 orders of magnitude smaller than the cavity size, they hardly change the R/Q value. The resonant frequency is most sensitive to errors in the cavity radius and reentrant depth. The error of the coupling structure in the Z direction causes the largest change in the Q_{ext} parameter.

TABLE I. Optimized dimensions and simulation results of the BAM pickup.

Parameters	Values
L_{cavity} (mm)	22.0
R_{cavity} (mm)	21.0
L_{gap} (mm)	6.4
R_{gap} (mm)	8.0
R_{pipe} (mm)	6.0
Frequency (GHz)	4.76
Q_0	1087.1
Q_{ext}	57.2
Q_l	54.3
$R/Q(\Omega)$	293
Sensitivity (peak voltage) (mV/pC)	131.2

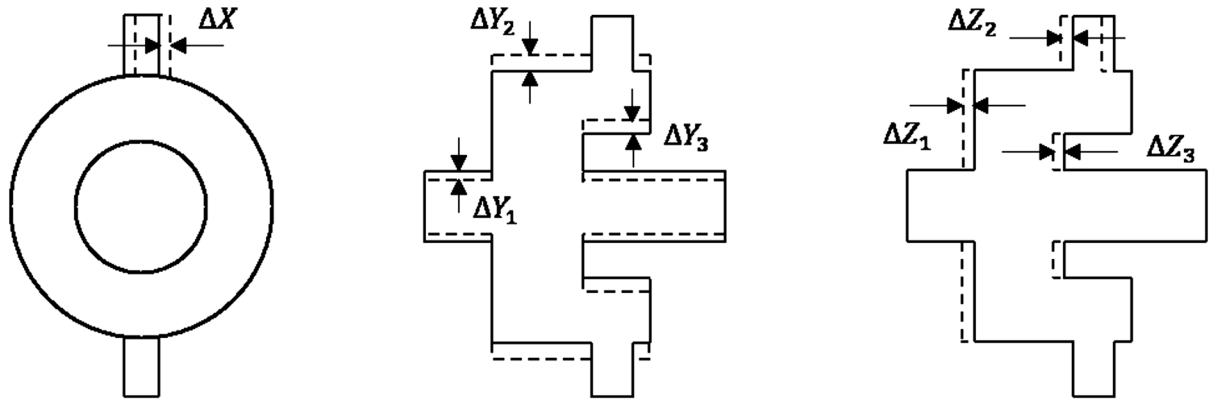

FIG. 4. Mechanical errors in three dimensions.

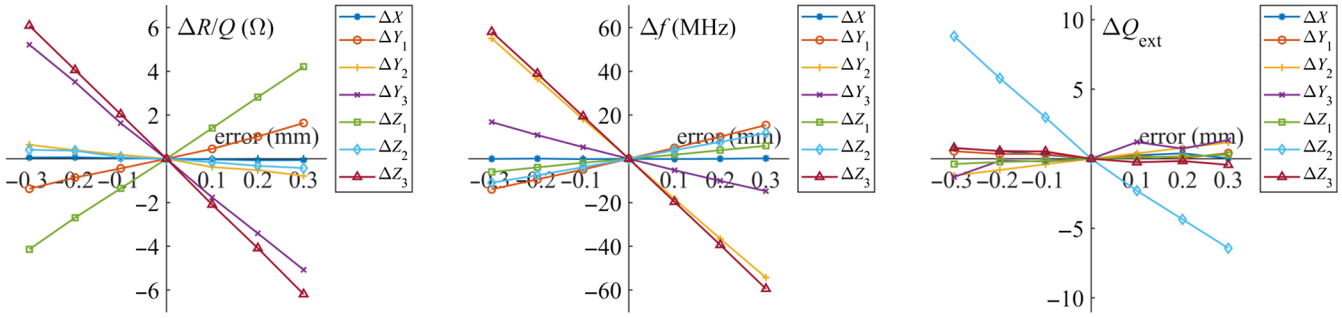

FIG. 5. rf parameter variations of TM_{110} mode from the tolerance analysis.

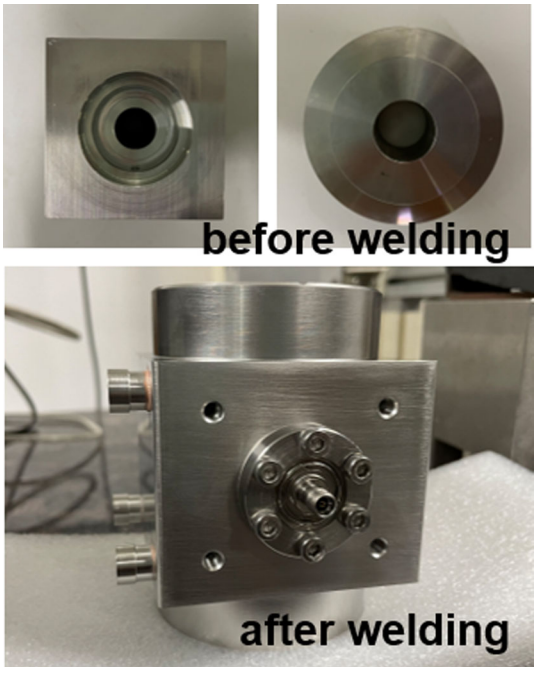

FIG. 6. BAM prototype: two parts of the pickup body and the assembly after welding.

C. Cold test result

Two pickups were fabricated to validate the simulation results. The cavity body made of stainless steel was composed of two pieces for the convenience of tuning before welding. The feedthroughs and antennas were designed as disassembled structures. Figure 6 shows pictures of the two main parts and the pickup after welding.

Before welding, a first rf measurement using a network analyzer and cavity tuning based on the tolerance analysis in Sec. II B was performed. The cavity length and gap length were selected as tuning parameters, which are easy to adjust and have little impact on the quality factor. In the tuning process, we reduced the gap length to increase the resonant frequency or reduced the cavity length to decrease the frequency. The cavity tuning accuracy in the fabrication process was 10 μm. The difference between the frequency after tuning and the target frequency was within 1 MHz. Afterward, the pickups were welded and measured again in the laboratory. The rf parameters of two pickups before and after welding are summarized in Table II. It can be seen from Table II that the change in quality factors in the welding process is very small. However, the process has a great influence on the resonant frequency. Especially, for pickup 2, the frequency shift caused by welding is 0.87 MHz.

TABLE II. Cold test results of two pickups.

BAM pickup	Frequency (MHz)	Q_0	Q_{ext}	Q_l
Before welding				
Pickup 1	4759.47	1030.9	60.0	56.7
Pickup 2	4760.63	1020.2	53.2	50.6
After welding				
Pickup 1	4759.12	1015.7	60.5	57.1
Pickup 2	4761.50	1033.8	54.2	51.5

III. BAM ELECTRONICS

For cavities with a low loaded Q factor Q_l, the bandwidth of the rf signal is relatively wide, which indicates a small decay constant [36]. The readout electronics mainly adopt the in-phase and quadrature (IQ) demodulation scheme, mixing the rf signal with a local oscillator (LO) to the baseband. The amplitude, A, and phase, Φ, can be easily obtained from the in-phase, $I(t)$, and quadrature phase, $Q(t)$, components [37]. The electronics prototype consists of three parts: an rf front-end, high-speed analog-to-digital converters (ADCs), and a digital signal processing board [38]. The rf front end produces the baseband signals from a raw signal. The baseband signals are sampled by high-speed ADCs and then processed in a field-programmable gate array (FPGA) board. The LO signal and the ADC sampling clock are locked to the reference clock.

The readout electronics system we developed for the BAM is shown in Fig. 7. In our design, the rf signal from the pickup is fed into a bandpass filter centered at approximately 4760 MHz, which can reject the high-order modes and reduce the noise. The filter is followed by a programmable attenuator and a low noise amplifier to extend the dynamic range. Since the machine reference system provides a reference signal at 2856 MHz, an LO synthesis module is added to the front end. The LO signal and an ADC sampling clock are generated in this module, and their phases can be adjusted by the FPGA board. Baseband signals from the front end are recorded by 16-bit ADCs with a 238 MHz sampling rate. Amplitude and phase information is calculated from the samples by the online processing system.

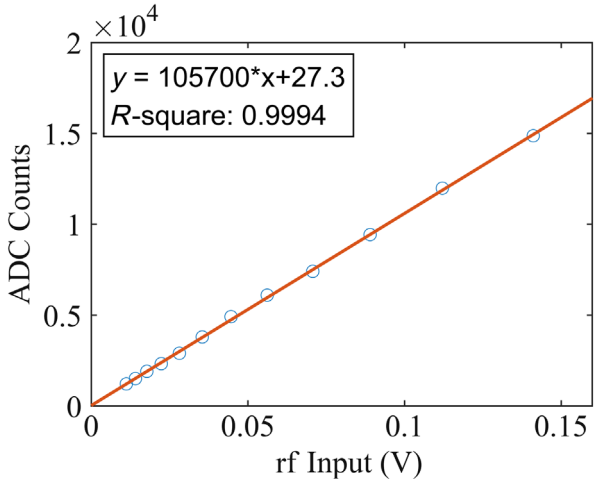

FIG. 8. Amplitude linearity test results of the electronics.

The rf front-end and digital motherboard are installed in a chassis. Temperature stabilization is employed inside the chassis. The temperature is controlled by a digital feedback loop, and the jitter is less than 0.05 °C rms. A low-noise power supply is integrated with the chassis, which reduces thermal drift and noise. The performance of the electronics was tested with rf signal generators before the beam experiments. We used two phase-locked signal generators to provide rf signal and reference signal, respectively. The amplitude of the output signal was recorded with an incremental rf input signal to measure the linearity. Figure 8 shows the linearity test result and the amplitude

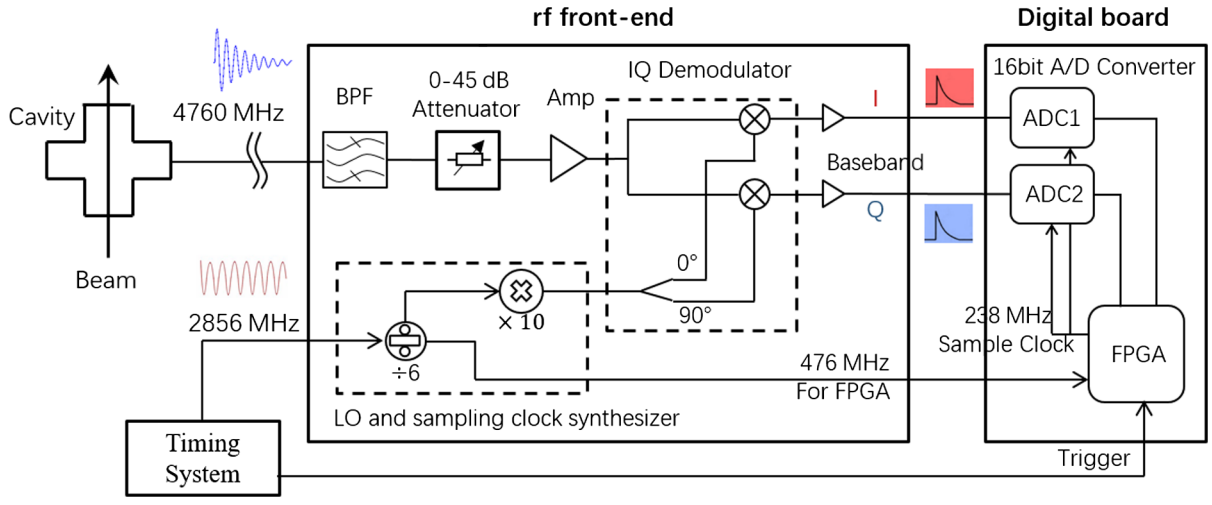

FIG. 7. Schematic diagram of the BAM electronics.

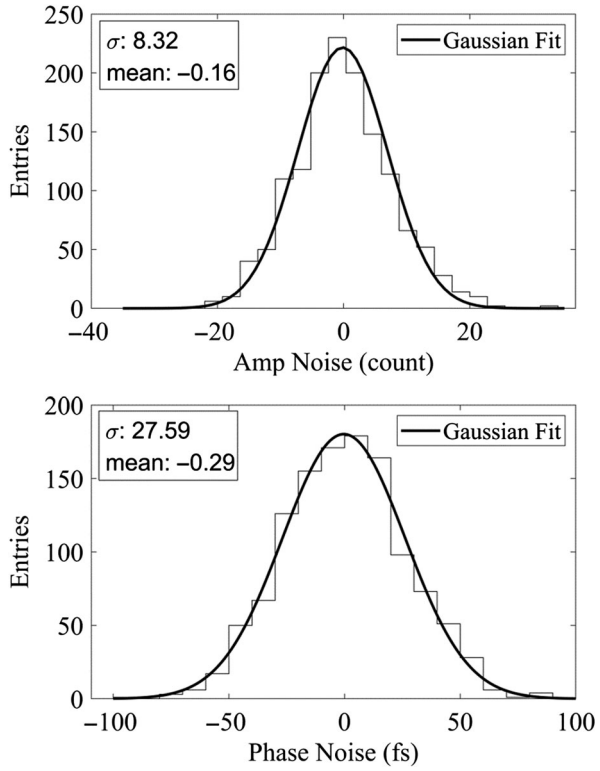

FIG. 9. Phase and amplitude errors of the electronics with a constant rf input.

linearity error is less than 1%. Afterward, the electronic noise was tested with a constant rf input voltage, about 80% of the full scale. As shown in Fig. 9, the amplitude error is 8.32 ADC counts, and the phase error is 27.59 fs@4760 MHz.

IV. EXPERIMENTAL RESULTS

The two pickups were installed downstream of the THz beamline at the Tsinghua Accelerator Laboratory. Figure 10 illustrates the layout of the THz beamline. The beamline consists of an S-band photocathode rf gun, an S-band accelerating tube, an undulator and a deflecting cavity. The distance between the two pickups is approximately 50 cm. The main beam parameters downstream of the beamline are summarized in Table III. In this section, we describe the signal processing method and the experimental results of the BAM.

The raw signal from the pickup was measured by an oscilloscope, and the bandwidth of the oscilloscope was

TABLE III. THz beamline beam parameters.

Parameters	THz beamline
Bunch charge (pC)	0.1–50
Bunch length (fs) (FWHM)	200
pulse repetition rate (Hz)	10
Electron energy (MeV)	33
Energy spread (rms)	0.15%

20 GHz. Figure 11 shows the measured rf signal and the simulated signal at 1 pC. In this figure, the peak voltage is measured to be approximately 130 mV/pC, and the decay constant is 3.5 ns. These measurements and simulation results are in good agreement.

As described in Sec. III, the rf signals are detected by down-conversion, and the baseband signals are sampled by ADCs. An example of the baseband signals is shown in Fig. 12(a). Because of the low Q_l factor, the pulses are relatively narrow compared to the sampling interval. The amplitude and the phase waveforms are calculated from the I, Q signals, as shown in Fig. 12(b). The sampled magnitude of the pulse is very sensitive to the sampling clock phase, and the top point of the magnitude waveform has the maximum signal-to-noise ratio. A feedback loop of the sampling clock is employed to sample the peak of the amplitude. The magnitude and phase of the peak point [Fig. 12(b)] are used for bunch charge and arrival time calculations, respectively.

The BAM charge reading was calibrated by comparing the amplitude of the signal to the charge read by adjacent integrating current transformer and stripline beam position monitors (SBPMs). The- calibration range was 0–1.2 pC. Figure 13 shows a good correlation between the ADC counts and the bunch charge. In this calibration procedure, the digital attenuator was set to 0 dB to provide the highest sensitivity. For higher charges, the attenuation value was reasonably set to guarantee a linear response in the electronics. The maximum charge in the experiments was approximately 50 pC.

The resolutions of arrival time and charge can be evaluated from the difference between the two BAM readings. Assuming that two BAMs have equal performance, the resolutions can be calculated as follows:

$$R_Q = \frac{\mathrm{std}(Q_1 - Q_2)}{\sqrt{2}} \tag{3}$$

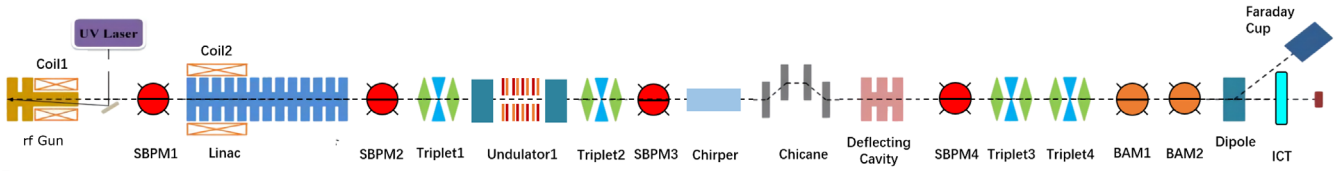

FIG. 10. Schematic diagram of the THz beamline.

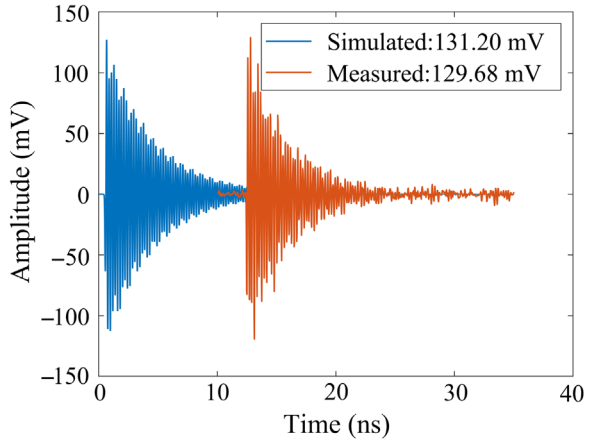

FIG. 11. Measured and simulated raw voltage signals from the pickup.

$$R_t = \frac{\mathrm{std}(t_1 - t_2)}{\sqrt{2}} \tag{4}$$

where Q_1, Q_2 are the bunch charges and t_1, t_2 are the bunch arrival times measured by two BAMs. The charge and arrival-time information were extracted by both BAMs over 1 min. In this measurement, the bunch charge was approximately 0.5 pC. The charges measured by the two BAMs are shown in Fig. 14(a), and the charge jitter is approximately 7.5 fC. Figure 14(b) shows the residual charge distribution. Therefore, the charge resolution of the BAM is 0.69 fC, calculated by Eq. (3). Figure 15(a) shows the arrival times measured by both BAMs. Both detectors show a slow drift of the arrival time, with a jitter of 250 fs. The difference between the two arrival times is plotted in

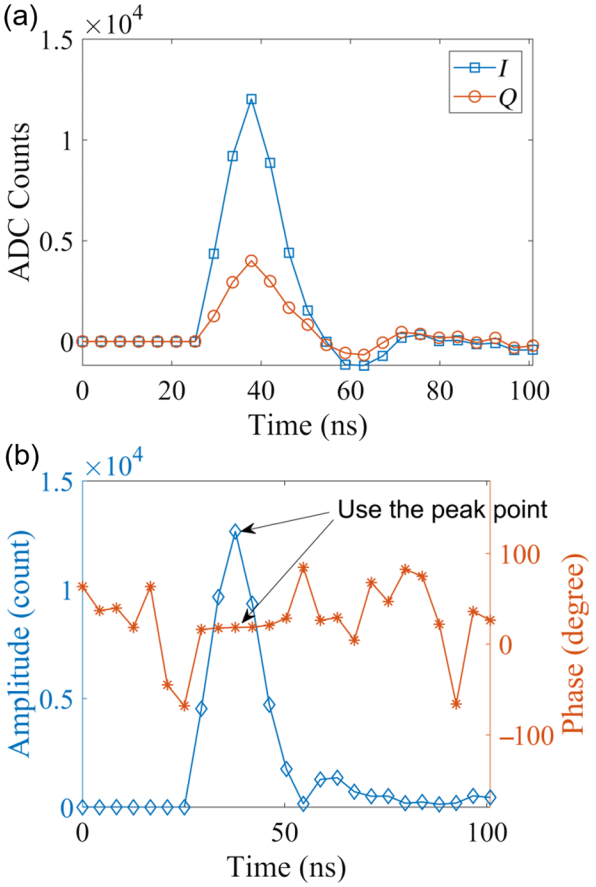

FIG. 12. Example of the baseband signals (a). Amplitude and phase waveforms calculated from the I, Q signals (b).

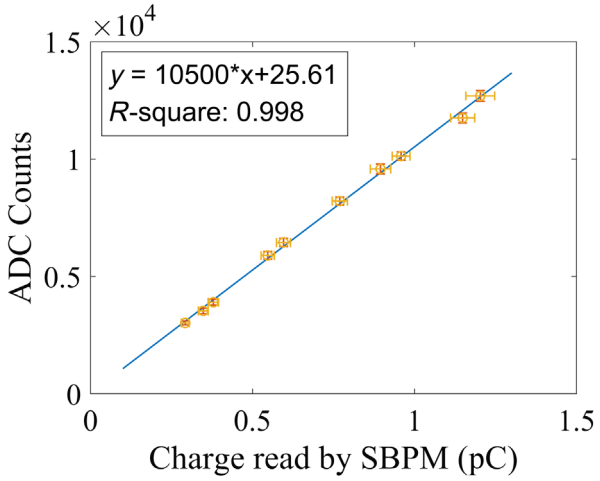

FIG. 13. ADC counts of the BAM vs charge read by the SBPM.

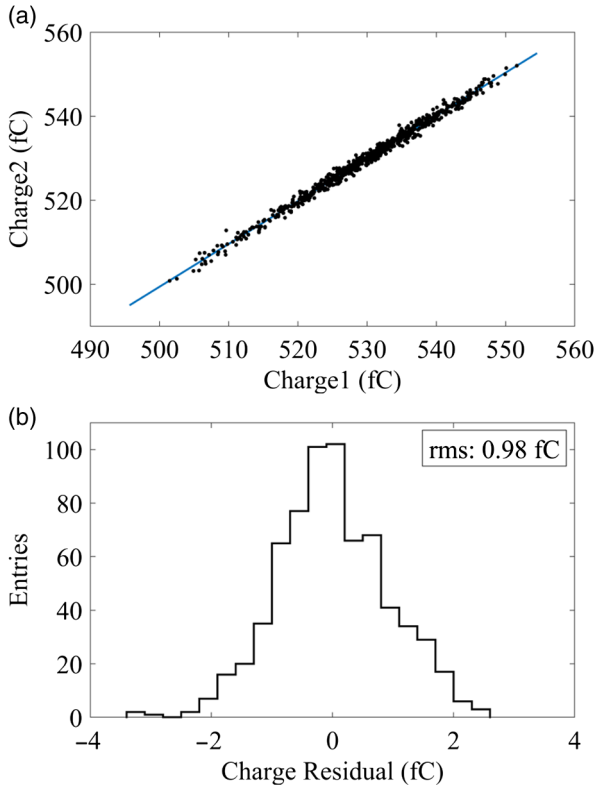

FIG. 14. Charges measured by two BAMs (a). Distribution of residual charge (b).

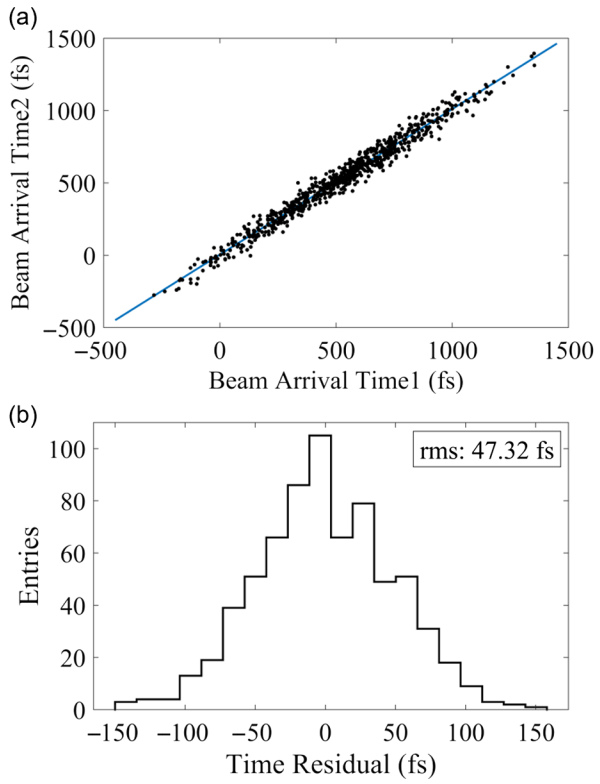

FIG. 15. Arrival times measured by two BAMs (a). Distribution of residual arrival time (b).

Fig. 15(b). Applying Eq. (4) results in an arrival-time resolution of 33.46 fs. The resolution values are slightly higher than the electronic noise described in Sec. III. One possible reason for the increased error is the high LO phase jitter from the synchronization system. However, any environmental noise could also cause poor performance. Finally, we measured the charge dependence of the beam arrival-time resolution. The relationship between the resolution and the charge is shown in Fig. 16. In this figure, the resolution between 50 and 0.5 pC slowly deteriorates from 30 to 35 fs. However, below 0.5 pC, it rapidly becomes worse. The resolution is approximately inversely proportional to the bunch charge, that is, mainly limited by the signal-to-noise ratio of the electronics.

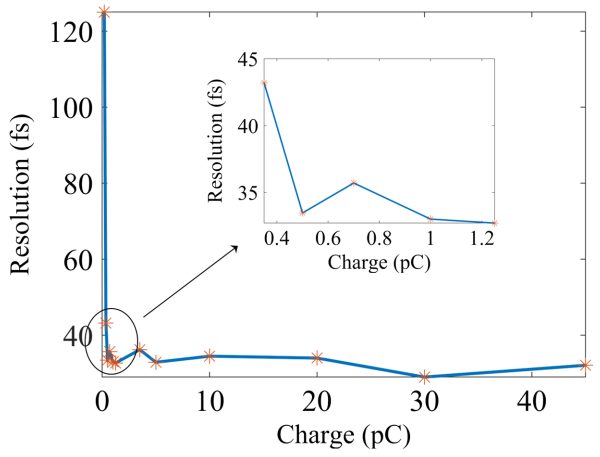

FIG. 16. BAM resolution dependence on the charge.

V. SUMMARY

Pump-probe experiments in FEL and UED facilities have an increasing demand for short and low charge bunches, where the timing jitter is specifically critical. We constructed a high-resolution cavity BAM system for bunch charges below 1 pC. A reentrant cavity at 4.76 GHz was designed. The R/Q parameter was optimized to realize the maximum sensitivity. The measurements agree well with the simulations. Two BAMs were arranged on the THz beamline at the Tsinghua Accelerator Laboratory, and the performance was evaluated by beam tests. The results show high resolutions of 33.46 fs and 0.69 fC with bunch charges of 0.5 pC. This performance is mainly limited by the BAM electronics and the LO signal from the synchronization system. Further studies on electronics are ongoing. Further experiments will hopefully achieve sub-10 fs resolution for charges less than 1 pC.

[1] K.-J. Kim, Z. Huang, and R. Lindberg, *Synchrotron Radiation and Free-Electron Lasers: Principles of Coherent X-Ray Generation* (Cambridge University Press, Cambridge, England, 2017).

[2] *X-Ray Free Electron Lasers—Applications in Materials, Chemistry and Biology*, edited by U. Bergmann, V. Yachandra, and J. Yano(The Royal Society of Chemistry, London, 2017).

[3] H. T. Lemke, M. Weaver, M. Chollet, J. Robinson, J. M. Glownia, D. Zhu, M. R. Bionta, M. Cammarata, M. Harmand, R. N. Coffee, and D. M. Fritz, Femtosecond optical/hard X-ray timing diagnostics at an FEL: Implementation and performance, in *Proceedings of SPIE Optics+Optoelectronics, 2013, Prague, Czech Republic* (2013), Vol. 8778, p. 87780S.

[4] R. Srinivasan, V. A. Lobastov, C.-Y. Ruan, and A. H. Zewail, Ultrafast electron diffraction (UED): A new development for the 4D determination of transient molecular structures, Helv. Chim. Acta **86**, 1761 (2003).

[5] F. Löhl, V. Arsov, M. Felber, K. Hacker, W. Jalmuzna, B. Lorbeer, F. Ludwig, K.-H. Matthiesen, H. Schlarb, B. Schmidt, P. Schmüser, S. Schulz, J. Szewinski, A. Winter, and J. Zemella, Electron Bunch Timing with Femtosecond Precision in a Superconducting Free-Electron Laser, Phys. Rev. Lett. **104**, 144801 (2010).

[6] P. Craievich, S. Di Mitri, M. Milloch, G. Penco, and F. Rossi, Modeling and experimental study to identify arrival-time jitter sources in the presence of a magnetic chicane, Phys. Rev. ST Accel. Beams **16**, 090401 (2013).

[7] E. A. Seddon, J. A. Clarke, D. J. Dunning, C. Masciovecchio, C. J. Milne, F. Parmigiani, D. Rugg, J. C. H. Spence, N. R. Thompson, K. Ueda, S. M. Vinko, J. S. Wark, and W. Wurth, Short-wavelength free-electron

laser sources and science: A review, Rep. Prog. Phys. **80**, 115901 (2017).
[8] S. Serkez, G. Geloni, S. Tomin, G. Feng, E. V. Gryzlova, A. N. Grum-Grzhimailo, and M. Meyer, Overview of options for generating high-brightness attosecond x-ray pulses at free-electron lasers and applications at the European XFEL, J. Opt. **20**, 024005 (2018).
[9] C. Feng and H.-X. Deng, Review of fully coherent free-electron lasers, Nucl. Sci. Tech. **29**, 160 (2018).
[10] J. B. Rosenzweig *et al.*, Generation of ultra-short, high brightness electron beams for single-spike SASE FEL operation, Nucl. Instrum. Methods Phys. Res., Sect. A **593**, 39 (2008).
[11] S. Reiche, P. Musumeci, C. Pellegrini, and J. B. Rosenzweig, Development of ultra-short pulse, single coherent spike for SASE x-ray FELs, Nucl. Instrum. Methods Phys. Res., Sect. A **593**, 45 (2008).
[12] W. Decking and T. Limberg, European XFEL post-TDR description, European XFEL GmbH, Hamburg, Germany, Technical Report No. XFEL.EU TN-2013-004, 2013.
[13] T. Tschentscher, Layout of the X-ray systems at the European XFEL, European XFEL GmbH, Hamburg, Germany, Technical Report No. XFEL.EU TR-2011-001, 2011.
[14] B. J. Siwick, J. R. Dwyer, R. E. Jordan, and R. J. D. Miller, Ultrafast electron optics: Propagation dynamics of femtosecond electron packets, J. Appl. Phys. **92**, 1643 (2002).
[15] J. C. Frisch, Beam arrival time monitors, in *Proceedings of IBIC2015, Melbourne, Australia, 2015* (JACoW, Geneva, Switzerland, 2016), pp. 256–262.
[16] F. Löhl, Optical synchronization of a free-electron laser with femtosecond precision, Ph.D. thesis, Hamburg University, Hamburg, Germany, 2009.
[17] M. K. Czwalinna, C. Gerth, H. Schlarb, and B. Steffen, Upgraded bunch arrival-time monitors for the European XFEL reaching below 3 fs time resolution, in *Proceedings of IBIC2019 in Malmö, Sweden* (unpublished).
[18] M. K. Bock, Measuring the electron bunch timing with femtosecond resolution at FLASH, Ph.D. thesis, Hamburg University, Hamburg, Germany, 2012.
[19] B. E. J. Scheible, S. Mattiello, A. Penirschke, M. K. Czwalinna, H. Schlarb, W. Ackermann, and H. De Gersem, Pickup development for short low-charge bunches in x-ray free-electron lasers, Phys. Rev. Accel. Beams **24**, 072803 (2021).
[20] M. K. Czwalinna, C. Gerth, H. Schlarb, S. B. Habib, S. Korolczuk, J. Szewiński, and A. Kuhl, New design of the 40 GHz bunch arrival time monitor using MTCA.4 electronics at flash and for the European XFEL, in *Proceedings of IBIC2013, Oxford, UK, 2013* (JACoW, Geneva, Switzerland, 2013), pp. 749–752, https://jacow.org/IBIC2013/papers/WEPC31.pdf.
[21] T. Schietinger *et al.*, Commissioning experience and beam physics measurements at the SwissFEL Injector Test Facility, Phys. Rev. Accel. Beams **19**, 100702 (2016).
[22] T. Weiland and R. Wanzenberg, Wake fields and impedances, in *Frontiers of Particle Beams: Intensity Limitations* (Springer, Berlin, Heidelberg, 1992), pp. 39–79.
[23] T. Nakamura, Development of beam-position monitors with high position resolution, Master's thesis, The University of Tokyo, 2008.
[24] A. Angelovski, M. Hansli, I. Dornmair, B. Zeitler, A. Penirschke, F. Grüner, and R. Jakoby, Pickup design for arrival-time measurements at REGAE, in *Proceedings of EAAC2013, Elba, Italy* (unpublished).
[25] J. Hong, J. Han, C. Kim, and H. Yang, Bunch arrival time monitor test at PAL-XFEL ITF, in *Proceedings of IPAC'16, Busan, Korea, 2016* (JACoW, Geneva, Switzerland, 2016), pp. 223–225.
[26] A. Brachmann *et al.*, Femtosecond operation of the LCLS for user experiments, in *Proceedings of IPAC'10, Kyoto, Japan, 2010* (JACoW, Geneva, Switzerland, 2010), pp. 2287–2289.
[27] S.-S. Cao, R.-X. Yuan, J. Chen, and Y.-B. Leng, Dual-cavity beam arrival time monitor design for the Shanghai soft X-ray FEL facility, Nucl. Sci. Tech. **30**, 72 (2019).
[28] H. Maesaka, S. Inoue, T. Ohshima, S. Matsubara, T. Shintake, and Y. Otake, Development of the rf cavity BPM of XFEL/spring-8, in *Proceedings of 9th European Workshop on Beam Diagnostics and Instrumentation for Particle Accelerators, DIPAC09, Basel, Switzerland* (JACoW, Geneva, Switzerland, 2009), pp. 56–58, https://jacow.org/d09/papers/MOPD07.pdf.
[29] M. Hansli, A. Angelovski, R. Jakoby, A. Penirschke, K. Flöttmann, D. Lipka, H. Schlarb, S. Vilcins, F. Grüner, and B. Zeitler, A Beam Arrival Time Cavity for REGAE at DESY, in *Proceedings of IPAC'14, Dresden, Germany, 2014* (JACoW, Geneva, Switzerland, 2014), pp. 1820–1822.
[30] CST Microwave Studio, Germany (2018), www.cst.com.
[31] S. Walston *et al.*, Performance of a high resolution cavity beam position monitor system, Nucl. Instrum. Methods Phys. Res., Sect. A **578**, 1 (2007).
[32] J.-H. Han, Dynamics of electron beam and dark current in photocathode RF guns, Ph.D. thesis, Hamburg University, Hamburg, Germany, 2005.
[33] H. Qian, Research on the emittance issues of photocathode rf gun, Ph.D. thesis, Tsinghua University, 2012.
[34] C. Simon, M. Luong, S. Chel, O. Napoly, J. Novo, D. Roudier, N. Rouvière, N. Baboi, N. Mildner, and D. Nölle, Performance of a reentrant cavity beam position monitor, Phys. Rev. ST Accel. Beams **11**, 082802 (2008).
[35] Q. Luo, B. Sun, and D. He, Design of s-band re-entrant cavity BPM, Nucl. Sci. Tech. **20**, 133 (2009).
[36] M. Stadler, R. Baldinger, R. Ditter, B. Keil, F. Marcellini, G. Marinkovic, M. Roggli, M. Rohrer, D. Lipka, D. Nölle, and S. Vilcins, Low-Q cavity bpm electronics for E-XFEL, FLASH-II and SWISS-FEL, in *Proceedings of. IBIC2014*, CA (JACoW, Geneva, Switzerland, 2014), Vol. 14, pp. 670–674, https://jacow.org/IBIC2014/papers/WEPD12.pdf.
[37] H. Maesaka, H. Ego, S. Inoue, S. Matsubara, T. Ohshima, T. Shintake, and Y. Otake, Sub-micron resolution rf cavity beam position monitor system at the SACLA XFEL facility, Nucl. Instrum. Methods Phys. Res., Sect. A **696**, 66 (2012).
[38] M. Stadler, R. Baldinger, R. Ditter, B. Keil, R. Kramert, G. Marinkovic, M. Roggli, D. Lipka, D. Nölle, M. Pelzer, and S. Vilcins-Czvitkovits, Beam test results of undulator cavity BPM electronics for the European XFEL, in *Proceedings of IBIC2012, Tsukuba, Japan* (JACoW, Geneva, Switzerland, 2012), pp. 404–408, https://jacow.org//IBIC2012/papers/TUPA27.pdf